Materials Research. 2023; 26:e20230204
DOI: https://doi.org/10.1590/1980-5373-MR-2023-0204

Solid State Recycling of Vanadis®8 Steel Scraps Using Powder Metallurgy

Pedro Henrique Gonçalves[a], *Agata Mayara Paula Pontes*[a], *Marcela Silva Lamoglia*[a], *Bruna Horta Bastos Kuffner*[a]*, *Antonio Augusto Araújo Pinto da Silva*[a], *Gilbert Silva*[a]

[a]*Universidade Federal de Itajubá (UNIFEI), Itajubá, MG, Brasil.*

Received: April 14, 2023; Revised: August 21, 2023; Accepted: September 01, 2023

Vanadis®8 is a high-value tool steel, that undergoes gas atomization and hot isostatic pressing during production , resulting in costly waste. Repurposing this waste material through powder metallurgy (PM) offers a cost-effective solution. This study explores the PM process applied to Vanadis®8 steel scraps, involving high energy ball milling, uniaxial pressing, and sintering. The final product and the as-received steel underwent heat treatments, including quenching and tempering. Microstructural evaluation employed X-ray diffraction and scanning electron microscopy, while physical evaluation entailed Archimedes density measurements. Mechanical analysis was carried out through microhardness and compression strength tests. Results revealed that optimal milling conditions were achieved at 30 hours with 400 rpm (s^{-1}). Vanadis®8 steel produced through PM attained 85% densification compared to the as-received material (6.31 g/cm^3). MC-type carbides were present in all evaluated conditions. Heat treatments improved mechanical values for all conditions, suggesting that PM-produced Vanadis®8 steel, subjected to quenching and tempering, presents a viable reuse option.

Keywords*: Vanadis®8 Steel, High Energy Ball Milling, Powder Metallurgy.*

1. Introduction

The metallurgical industry represents a significant energy and raw material consumer. An important portion of its waste consists of scraps, primarily originating from mechanical forming and machining processes. These concerns are rooted in the context of sustainable development[1,2]. In 2018, global steel scrap trade reached approximately 105.4 million tons, underscoring its integral role within the metallurgical sector. Notably, recycling costs are significantly lower than those associated with manufacturing new steel, presenting a positive influence on both environmental and economic dimensions[3].

The scarcity of raw materials coupled with the direct correlation between reduced energy consumption and mitigated environmental impact further underscores the significance of a circular economy (CE) approach[4,5]. The CE paradigm has gained substantial global attention as an innovative model linking economic advancement with enhanced natural resource efficiency. This transformative model seeks to shift from a linear to a circular economy, where waste and recycled materials constitute key resource inputs. By promoting recycling, reconditioning, and resource-efficient practices, the CE approach champions lasting sustainability[6].

The present study investigates the feasibility of high energy ball milling (HEBM) as an alternative method to recycle Vanadis 8 cold work tool steel scraps, ultimately aiming to retain its desired properties. Tool steels like Vanadis 8, widely employed in tool, mold, and die manufacturing, are recognized for their exceptional wear resistance, even under high-temperature conditions[7-9]. However, traditional recycling methods perpetuate the cycle of environmental impacts and high energy consumption due to the production of additional scraps during the remelting process[10,11].

Powder metallurgy (PM) emerges as a viable solution to repurpose metal scraps that would otherwise be discarded or remelted. The PM process, comprising powder production, pressing, and sintering stages[12], offers an efficient means of recycling. HEBM is proven to effectively produce metal powder from scraps, with potential for the formation of metal matrix composites (MMCs), where a ductile metallic matrix incorporates rigid ceramic reinforcement[13-15]. Notably, particulate reinforcements have demonstrated superior performance in MMCs, attributed to their effective homogenization capabilities[16,17].

Numerous studies have demonstrated the technical effectiveness of HEBM in processing various types of alloys. For instance, it has been successfully applied to low and extra low carbon steels[11], AISI 52100 steel[18], UNS S31803 duplex stainless steel[19], aluminum bronze[20], Ti6Al4V alloy[21], X22CrMoV alloy[22], and others. In these cases, the authors achieved the production of extremely fine powders with predominantly irregular morphology and submicrometric granulometry. Moreover, the resulting workpieces exhibited good densification after the sintering process.

Vanadis 8 Superclean, a cold work tool steel from Bohler-Uddeholm, distinguishes itself through its wear resistance, hardness, and toughness combination. The uniform distribution of vanadium-rich MC-type carbides[23,24], achieved through the unique powder metallurgy process, contributes significantly to its mechanical strength. This contrasts with conventional casting processes that often result in inhomogeneous microstructures and mechanical properties due to primary

*e-mail: brunakuffner@hotmail.com

carbide growth and element segregation[25,26]. Vanadis 8, commercially available as plates and billets, undergoes annealing and subsequent heat treatment to achieve desired hardness and microstructural characteristics. It is likely that Barbedo et al.[27] and Toboła and Łętocha[28] offer additional insights into the processes of heat treatment and the resulting microstructures of Vanadis®8 steel.

In this context, our research aims to explore the potential of HEBM for recycling Vanadis 8 steel scraps while maintaining its core properties. By investigating aspects such as densification, microstructure, and mechanical properties, the study seeks to determine optimal HEBM parameters to achieve material parity with the original. The broader goal is to evaluate the viability and efficacy of HEBM in recycling Vanadis 8 steel scraps, preserving its essential attributes.

Table 1. Chemical composition of Vanadis®8 steel.

Chemical Composition (% wt.)					
C	Si	Mn	Cr	Mo	V
2.30	0.40	0.40	4.80	3.60	8.00

Table 2. Parameters used in Vanadis®8 steel scraps HEBM.

Milling Parameters	Value
Speed	350 - 400 rpm (s^{-1})
Ball to powder ratio	20:1
Time	10, 20, 30 hours
Downtime	15 minutes/hour
Shielding gas	Argon N5

2. Materials and Methods

2.1. Experimental route

The material utilized in this research is Vanadis®8 tool steel, specifically the annealed billet variant manufactured by Bohler-Uddeholm. The chemical composition of this steel, as provided by the manufacturer, is presented in Table 1.

The machining of the billet was conducted without the use of lubricating oils to prevent contamination. The machining parameters employed included a low feed of 40 rpm (s^{-1}) to minimize oxidation, a cut velocity of 70 m/min, and a depth of cut of 2 mm. Through binocular stereoscopic evaluation using an Olympus® SZ61 microscope, it was determined that the average thickness of the generated scraps was 1.4 mm.

For the subsequent process, 30 g of scraps were placed inside stainless steel jars along with 600 g of AISI 52100 steel spheres with three different diameters: 21 mm, 13 mm, and 8 mm. This amount of scraps was sufficient to produce the required samples for analysis. Argon gas with a purity of N5 (99.999%) was introduced into the jars to prevent oxidation of the scraps during the milling process. The HEBM was performed using a Noah-Nuoya® NQM 0.2 L planetary ball mill from Yangzhou Nuoya Machinery CO. In order to define the milling parameters a preliminary analysis was performed and the conditions evaluated are presented in Table 2. The powders were collected from the mill at regular intervals of 10, 20, and 30 hours of milling. According to results that will be discussed in section 4.1, only the condition of 30 hours/400 rpm (s^{-1}) was selected for subsequent use.

After milling, 3.4 grams of powder were separated for each sample. A metal matrix with a diameter of 8 mm was used, along with a Schulz® 30-ton uniaxial press, applying a compaction load of 490 MPa. The final mass and dimensions of each sample were measured to determine the green density.

Next, the samples underwent heat-treatments. Initially, they were sintered using a Nabertherm® HT04/17 tubular furnace with a controlled atmosphere of analytical argon flow. The heating rate was set at 5°C/min up to 450°C, and the temperature was held for 60 minutes. Subsequently, the temperature was increased to a rate of 15°C/min up to 1250°C, and the samples were held at that temperature for 90 minutes before being cooled inside the furnace.

For the quenching and tempering heat-treatments, a Brasimet® PXW-5 furnace was utilized. During quenching, the samples were heated up to 1080°C and held at that temperature for 30 minutes before being cooled in oil. The double tempering process was carried out at 520°C, with a soaking time of 120 minutes, followed by water cooling. These parameters were applied in accordance with the temperature and time ranges recommended by the Uddeholm technical catalog.

2.2. Microstructural characterization

To evaluate the morphology, distribution, and average size of the particles, the following techniques and equipment were employed. The phases were identified and analyzed using a Panalytical® X'Pert PRO X-ray diffractometer, utilizing Cu-Kα radiation with a scan angle of 30 to 90°, a step size of 0.02°, and a time per step of 1.5 seconds. In addition to phase identification, a Rietveld refinement was performed to determine the volumetric fraction of the identified phases using Gsas software. The crystallite size was calculated using the Scherrer equation ($D = K\lambda / \beta L cos\theta$), where D represents the crystallite size (in nm), K is Scherrer's constant (which varies based on crystal symmetry, and in this work, a value of 0.9 was adopted), λ is the wavelength of radiation (CuKα = 0.15442 nm), βL is the half-height width (FWHM) of the peaks for each phase, and θ is the Bragg diffraction angle in radians[29].

A Carl Zeiss® EVO MA15 scanning electron microscope was utilized in the secondary electron (SE) mode to evaluate the morphology and distribution of particles, and in the backscattered electron (BSE) mode to analyze the present phases.

The particle distribution and mean particle size were determined using a Microtrac® Bluewave S3500 laser granulometer. Subsequently, the powders were selected using a 100 mesh sieve (150 µm) in a Bertel electromagnetic stirrer, operating at a frequency of 10 Hz for 8 seconds. The metallic productivity was calculated based on the amount (in grams) of powders with a granulometry smaller than 150 µm. The porosity was determined using the results of the apparent density and the average of five images taken in predefined regions of the sample using an optical microscope, with the assistance of Olympus® Stream Basic 1.9.1 software.

2.3. Mechanical characterization and density measurements

For the mechanical characterization, microhardness and compression strength tests were conducted. The microhardness

was assessed using a Digimess® microhardness tester, specifically the Tester HV 1000 model. The testing involved applying a load of 0.5 kg (4.9 N) with an indentation time of 15 seconds. Ten indentations were made per sample, and the average values were calculated. Compression testing was performed on an Instron® 8801 universal testing machine with a capacity of 100 kN. The test was carried out following the ASTM E9-09 standard[30], which provides guidelines for determining the compression strength of metallic materials. In terms of physical characterization, density evaluation was conducted using the Archimedes principle, as specified in the ASTM C20-22 standard[31]. This standard outlines the procedure for measuring the density of solid materials using the Archimedes method.

3. Results and Discussion

3.1. Previous analysis parameters

Figure 1 in the study presents a stereoscope image of the Vanadis®8 steel scraps obtained after machining. The image shows that the scraps exhibit a helical morphology, which is typically associated with low cutting speeds and high plastic deformation resulting from shear stress[32]. The average length of the scraps is observed to be approximately 10 mm.

The subsequent study aimed to identify the optimal milling parameters (rotation and time) and the percentage of particles with a size below 150 µm. Powders with such characteristics are considered ideal for minimizing the porosity and enhancing the densification during the sintering process[33]. Figure 2 displays the volume percentage (%m) of powders with a granulometry greater than 150 µm after sieving, categorized according to the different milling parameters.

Rotation speed is indeed a crucial parameter for particle size reduction. In the initial milling stage (10 hours), a rotation speed of 400 rpm (s^{-1}) resulted in a volumetric fraction of powders with a granulometry smaller than 150 µm of 76 vol.%, which is higher compared to 30 hours at 350 rpm (s^{-1}), where a volumetric fraction of 61 vol.% was obtained. The milling speed is directly linked to the kinetic energy of the system. Increasing this parameter leads to more intense collisions between the milling spheres and the material inside the jar, as noted by Suryanarayana[15].

Indeed, the findings of Gheisari et al.[34] support the relationship between rotation speed and the kinetic energy of the system during milling. Their analysis demonstrated that increasing the rotation speed from 350 to 400 rpm (s^{-1}) led to a 14% increase in collision speed and a 31% increase in kinetic energy per shock for a Fe-45%Ni alloy. This further supports the understanding that higher rotation speeds result in more intense collisions and increased kinetic energy during the milling process.

The analysis of particle size evolution at a rotation speed of 400 rpm (s^{-1}) revealed a negligible decrease in granulometry from 10 to 30 hours of milling. For the 10 hour milling duration, the average particle size was found to be 60 µm, while for the 30 hour duration, the average size decreased to 20 µm. This result aligns with the expectations of HEBM, as longer milling times tend to result in a reduction in particle size. Based on these findings, the condition of 30 hours/400 rpm (s^{-1}) was selected as the best condition for subsequent use.

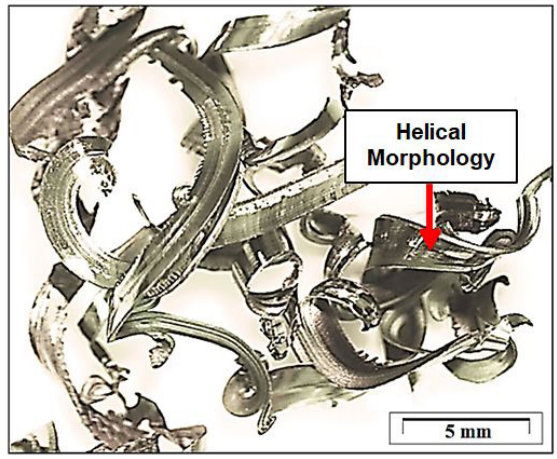

Figure 1. Stereoscope micrograph of Vanadis®8 steel scraps after machining.

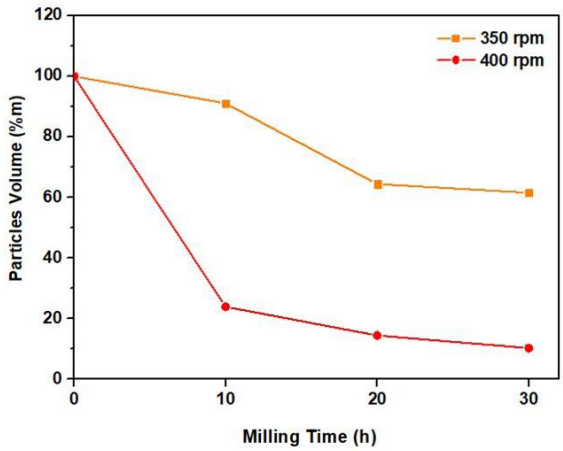

Figure 2. Volumetric mass fraction of powders with granulometry higher than 150 µm after HEBM.

3.2. Powder evolution analysis during milling

The morphology, size distribution, and amorphization of Vanadis®8 steel powder were analyzed up to 30 hours of milling at 400 rpm (s^{-1}). Figures 3 and 4 depict SEM/SE micrographs and particle size distribution obtained through laser granulometry analysis. After 10 hours of milling, a high volume of irregular particles was observed (Figure 3a). Analysis of the laser granulometry data (Figure 4a) revealed a bimodal distribution, with the presence of fine particles averaging 11 µm in size (representing 18% of the total volume of particles) and coarse particles averaging 47 µm in size (representing 82% of the total volume of particles).

With an increase in milling time to 20 hours, the morphology of the particles continued to exhibit irregular shapes (Figure 3b). Regarding granulometry analysis (Figure 4b), an asymmetric trimodal distribution was observed. The distribution consisted of fine particles with an average size of 4 µm (representing 2% of the total volume), medium

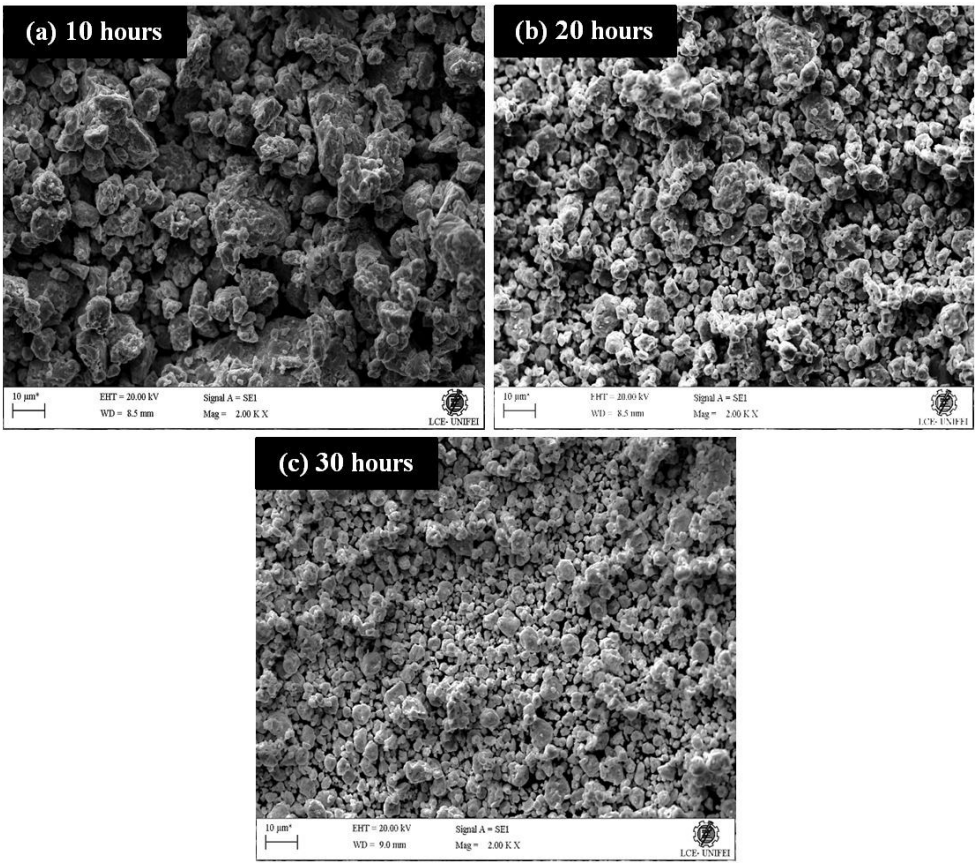

Figure 3. Morphology of Vanadis®8 steel particles after (a) 10 hours (b) 20 hours (c) 30 hours.

particles with an average size of 11 µm (representing 60% of the total volume), and coarse particles with an average size of 36 µm (representing 38% of the total volume).

After 30 hours of milling, the selected duration for subsequent processes, the particles maintained their irregular morphology (Figure 3c), and underwent a more significant reduction in size. Granulometric analysis (Figure 4c) confirmed an asymmetric trimodal distribution. Fine particles had an average size of 3 µm (representing 5% of the total volume), medium particles had an average size of 11 µm (representing 69% of the total volume), and coarse particles had an average size of 43 µm (representing 25% of the total volume).

The granulometry of the Vanadis®8 steel powder obtained through HEBM was found to be lower than that of Vanadis 4 steel powder produced by gas atomization, as reported in studies by Tornberg and Fölzer[35], Chang et al.[36], and Huang et al.[37]. This finding is considered highly promising, as HEBM is regarded as an excellent alternative to atomization[38]. Overall, an increase in milling time from 20 to 30 hours resulted in the identification of irregular particles with smaller granulometry. In both cases, an asymmetric trimodal granulometric distribution was observed.

Figure 5 illustrates the X-ray diffractograms of Vanadis®8 steel under different conditions: as received (bulk, in the annealed state), and after the HEBM process (powder) for 10, 20, and 30 hours (Figure 5a). The diffractograms reveal peaks corresponding to Fe-α phase and vanadium carbide (VC). The higher intensities of the Fe-α phase peaks can be attributed to the higher volumetric fraction of this phase (81%) and the planar density of the crystallographic planes. Based on the diffractograms of the samples subjected to HEBM, it can be concluded that there was no inherent contamination from the process. Furthermore, if any intermetallics were formed, their content was less than 3% and could not be detected by XRD. The observed differences were primarily in the width and intensity of the peaks. Similar observations of amorphization in different materials subjected to HEBM have been reported by authors such as Suryanarayana[39]. Additionally, less intense peaks, such as the VC peaks at 37º and 44º, were no longer discernible.

The reduction in peak intensity and broadening observed in Figure 5b after HEBM, compared to the as-received material, becomes more pronounced with longer processing times. These changes are attributed to severe non-uniform plastic deformations of the crystalline lattice, resulting in microstrain, crystalline defects, and reductions in crystallite size. Additionally, a leftward shift of the peaks can be observed, which is again a consequence of the plastic deformation imposed on the system during HEBM[19,40].

These findings gain additional support through the examination of crystallite sizes pertaining to the Fe-α and VC phases within Vanadis®8 steel (depicted in Figure 5c). It is evident that during the 10 to 20-hour milling period, there is a notable 28% reduction in crystallite size for the Fe-α phase,

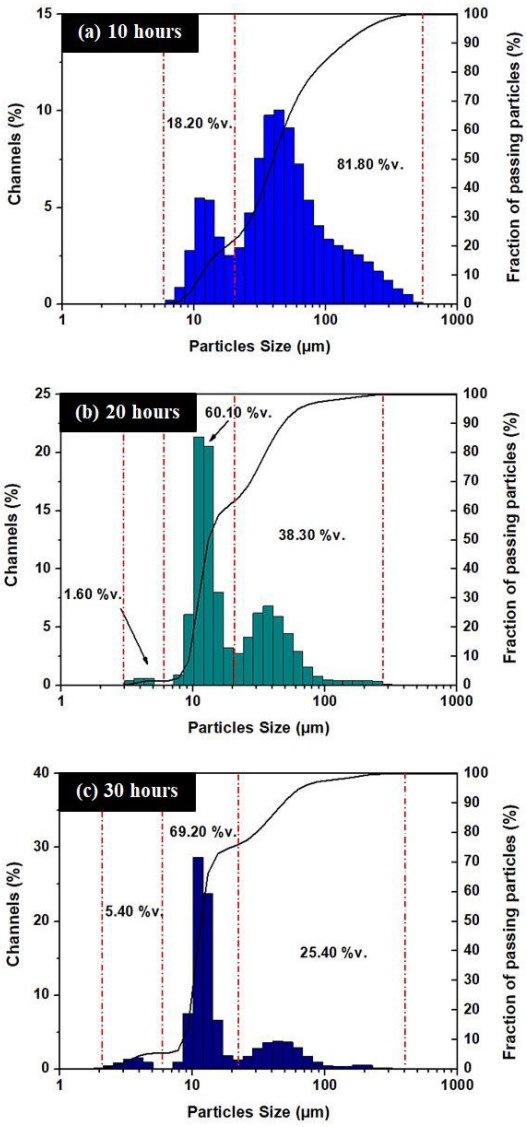

Figure 4. Granulometric distribution of Vanadis®8 steel particles after (a) 10 hours (b) 20 hours (c) 30 hours.

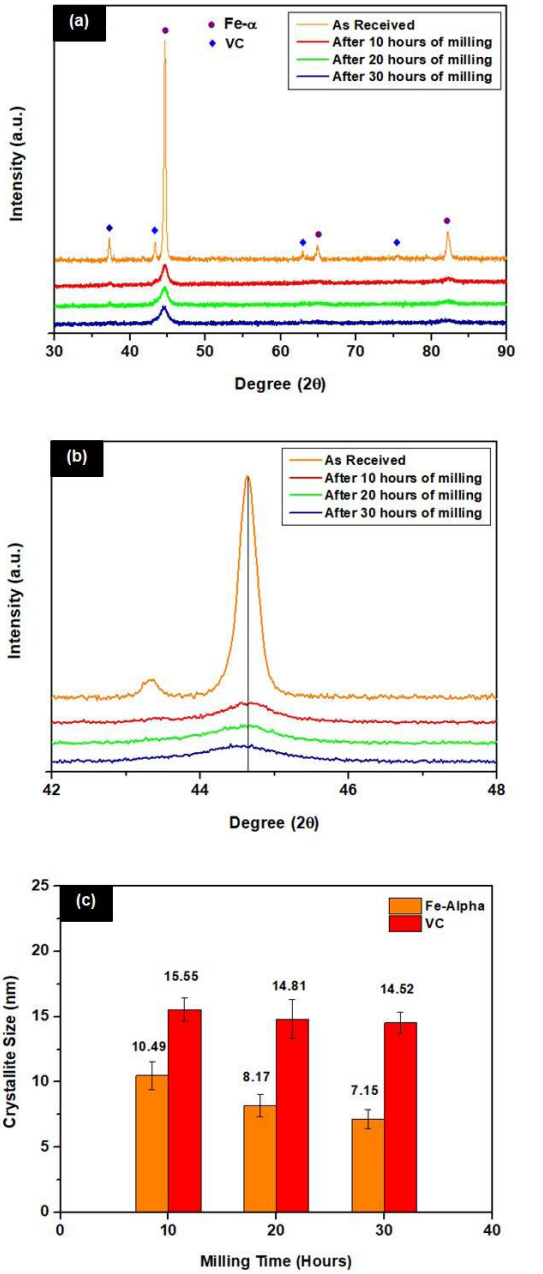

Figure 5. Analysis via X-ray diffraction of Vanadis®8 steel (a) Phases present in Vanadis®8 steel under as-received conditions (annealed state, bulk) and after HEBM for milling times of 10, 20 and 30 hours (powder) (b) Reduction in intensity and broadening of the peaks after HEBM, when compared to the material as received (c) Crystallite size of the phases after HEBM.

alongside a 5% decrease for the VC phase. Subsequently, as the milling duration extends from 20 to 30 hours, a further decline in crystallite size is observed, measuring 14% for the Fe-α phase and 2% for the VC phase. On a comprehensive scale, encompassing the 10 to 30-hour interval, a significant 47% reduction in crystallite size is demonstrated for the Fe-α phase, with a corresponding 7% decrease for the VC phase. These progressive diminishments over prolonged milling durations are attributed to the concurrent processes of amorphization and the development of solid solutions.

3.3. Recycled material characterization

3.3.1. Densification and microstructure after heat-treatments

The densification results for Vanadis®8 produced by PM are summarized in Table 3. Prior to the sintering process, the material exhibited a density of 4.82 g/cm^3. After sintering, the density escalated to 6.31 g/cm^3, as determined by the Archimedes method, marking a substantial 31% upsurge from its initial green state.

Comparing the density after sintering with the manufacturer-provided density of 7.46 g/cm^3 for the material produced by hot isostatic pressing (HIP), it can be observed that the Vanadis®8 produced by PM achieved 85% of the densification of the as-received material (relative density after sintering

of 0.85). The apparent porosity value was found to be 13%, and the volumetric shrinkage was 26%. Overall, the results demonstrate a significant reduction in porosity after sintering, which can be considered satisfactory depending on the desired application, as the value obtained is close to that of the forerunner material.

Figure 6 presents SEM/BSD micrographs of Vanadis®8 steel in different conditions: as received, as received quenched and tempered twice, after sintering, and after sintering, quenched and tempered twice. In the as received condition (Figure 6a), a small volume of pores can be observed, along with homogeneously distributed MC-type carbides in a ferritic matrix with average size of 1 µm. After quenching and tempering twice (Figure 6b), the micrograph shows the presence of MC-type carbides uniformly dispersed in a matrix consisting of tempered martensite.

In the micrographs of Vanadis®8 steel after sintering (Figure 6c), a microstructure with fine VC-type carbides dispersed in a ferritic matrix can be observed. The micrographs do not reveal the formation of secondary carbides or the dissolution of MC-type carbides, indicating the material's stability at high temperatures. Any solid solutions or intermetallic phases that may have formed during HEBM are present in small percentages, making them difficult to identify. Furthermore, the micrographs distinctly illustrate a notable refinement in the grain size of the MC-type carbides. Upon comparing Figure 6b with Figure 6d, a discernible reduction in carbide dimensions within Figure 6d becomes apparent, attributed to the influence of the HEBM process.

Despite the efforts to control powder size and distribution, it is important to note that the occurrence of pores within the material remains inevitable due to the inherent nature of the PM technique. Following the sintering process, coupled with two subsequent cycles of quenching and tempering (Figure 6d), the material exhibited a microstructure similar to that observed in Figure 6c, with the presence of fine MC-type carbides distributed in a tempered martensite (α'_R) matrix instead of a ferritic matrix. The observations rendered by the micrographs find validation through the diffractogram displayed in Figure 7.

The diffractogram of Figure 7 shows the phases present in the material after different heat treatments. After sintering, the peaks corresponding to ferrite (α) and MC primary carbides are observed. Following sintering, quenching, and double tempering, in addition to the peaks of MC primary carbides, the presence of martensite (α') can be identified. After the double temper heat treatment, only the peaks of tempered martensite and MC-type carbides are observed. The identification of the martensite peaks was based on the

Table 3. Densification results obtained for Vanadis®8 steel produced by PM.

Physical Property	Average Values
Density before sintering (g/cm^3)	4.82
Density after sintering (g/cm^3)	6.31
Apparent porosity (%)	13
Relative density after sintering	0.85
Volumetric shrinkage (%)	26

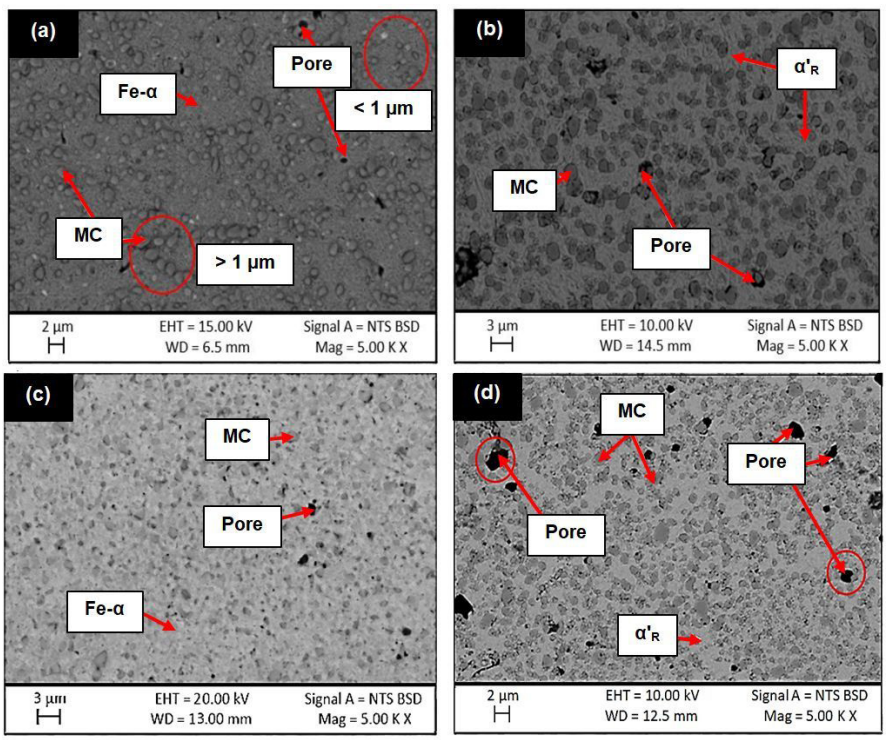

Figure 6. Micrographs (SEM/BSD) of Vanadis®8 steel (a) As received (annealed) (b) As received, quenched and tempered twice (c) Sintered (d) Sintered, quenched and tempered twice.

Table 4. Mechanical properties of Vanadis®8 steel as received (annealed), as received quenched and tempered, sintered, and sintered, quenched and tempered twice.

Mechanical Property	As Received (Annealed)	As Received, Quenched and Tempered Twice	Sintered	Sintered, Quenched and Tempered Twice
Microhardness HV (kgf/mm^2)	274	812	186	847
Elastic Modulus (GPa)	230*	/	10	17
Compressive strength (GPa)	/	/	1326	1410

*Bohler-Uddeholm[25]

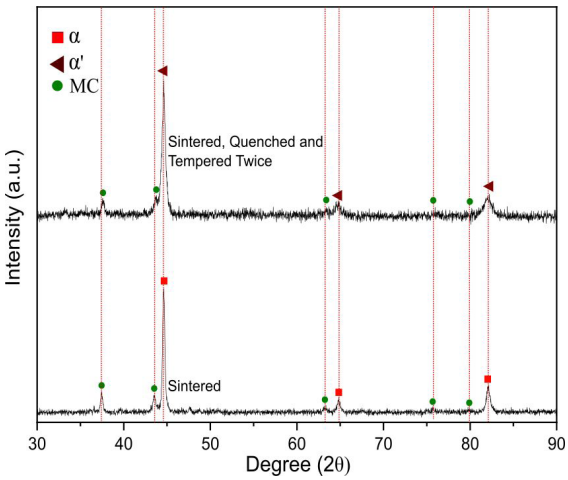

Figure 7. XRD diffractograms of Vanadis®8 steel in sintered and sintered, quenched and tempered twice conditions along with the phase identification.

lattice parameters identified by Gonzalez-Pociño et al.[41] and Sobotova[42], as well as the analyses performed by SEM and microhardness. The main peak (110) of martensite, located near the 45° angle, confirms that both the martensite and alpha phases have the same diffraction angle, but they can be differentiated by their tetragonality and the ratio of the c/a lattice parameter.

3.3.2. Mechanical characterization

The microhardness and elastic modulus results for Vanadis®8 steel under different conditions are presented in Table 4. The sintered material exhibited 68% of the microhardness compared to the as-received material. However, following quenching and tempering heat treatments, both the as-received and sintered Vanadis®8 steel showed a significant increase in microhardness. The microhardness values obtained for both conditions were closely aligned with a difference of only 4%. These findings indicate that the microhardness of the material processed via PM and subsequently heat-treated is akin to that of the as-received material subjected to heat treatment.

The elastic modulus results were analyzed across various conditions. Notably, the as-received material underwent quenching and tempering, resulting in an elastic modulus of 230 GPa, as obtained from Uddeholm technical catalog. The sintered material and the sintered, tempered, and annealed sample displayed considerably lower elastic modulus of 10 GPa and 17 GPa, respectively, based on experiments conducted in this study. Comparing these results, it is evident that the elastic modulus values were notably affected by the processing conditions. The sintered material exhibited only 4.3% of the elastic modulus of the as-received, quenched, and tempered material. The findings resonate with observations in studies conducted by Kuffner et al.[18] and Matos et al.[22]. For instance, in Kuffner et al.'s work[18], the sintered material's elastic modulus relative to the cast material amounted to a mere 1%. Similarly, Matos et al.[22] examined the reutilization of the X22CoMoV12-1 alloy and found that the average elastic modulus of the developed materials accounted for 2.07% of the cast material. The compressive strength of the Vanadis®8 steel specimens was also evaluated to understand the material's response under different processing conditions. The results revealed a notable increase in compressive strength following the sintering process, with an average value of 1326 MPa for the sintered samples. Subsequent application of quenching and tempering heat treatments led to a further enhancement in compressive strength, resulting in an average value of 1410 MPa for the sintered, tempered, and annealed specimens.

4. Conclusions

The present study evaluates the feasibility of reusing waste material from Vanadis®8 steel production through PM. The optimized milling process, particle evolution analysis, and characterization of the recycled material contribute to the understanding of the potential benefits of this approach.

The analysis of milling parameters revealed that a rotation speed of 400 rpm (s-1) for 30 hours achieved particle size reduction, leading to particles with smaller granulometry. X-ray diffraction confirmed that the powder did not experience significant contamination during milling and displayed amorphization tendencies. The microstructural analysis revealed finer carbides and reduction in crystallite size with increasing milling time, confirming the effects of amorphization and solubilization.

The recycled Vanadis®8 steel produced by PM achieved 85% densification compared to the as-received material, exhibiting reduced porosity and enhanced mechanical properties. The microstructure of the sintered material displayed fine carbides within a ferritic matrix, indicating stability at high temperatures. Quenching and tempering treatments significantly improved microhardness, with values closely matching those of the as-received material subjected to the same treatments.

In conclusion, repurposing waste material from Vanadis®8 steel production through PM has been established as a viable technical alternative to its conventional production methods.

5. Acknowledgments

The authors would like to thank CAPES for financing this research and the company Bohler-Uddeholm for donating the material.

6. References

1. Steinfeld A, Meier A. Solar fuels and materials. In: Cleveland CJ, editor. Encyclopedia of energy. Amsterdam: Elsevier Science; 2004. p. 623-37.
2. Ferronato N, Torretta V. Waste mismanagement in developing countries: a review of global issues. Int J Environ Res Public Health. 2019;16(6):1060. http://dx.doi.org/10.3390/ijerph16061060.
3. Reijonen J, Jokinen A, Puukko P, Lagerbom J, Lindroos T, Haapalainen M, et al. Circular economy concept in additive manufacturing. 1st ed. Milan: European Powder Metallurgy Association; 2017.
4. Hagelüken C, Goldmann D. Recycling and circular economy: towards a closed loop for metals in emerging clean technologies. Miner Econ. 2022;35(3-4):539-62.
5. Yang M, Chen L, Wang J, Msigwa G, Osman AI, Fawzy S, et al. Circular economy strategies for combating climate change and other environmental issues. Environ Chem Lett. 2023;21(1):55-80.
6. Fatimah YA, Kannan D, Govindan K, Hasibuan ZA. Circular economy e-business model portfolio development for e-business applications: impacts on ESG and sustainability performance. J Clean Prod. 2023;415:137528-40.
7. Højerslev C. Tool steels. 1st ed. Roskilde: Risø National Laboratory; 2001.
8. Roberts G. A tool steels. 5th ed. Materials Park: ASM International; 1998.
9. Tański T, Labisz K, Brytan Z, Jonda E, Sroka M. Thermal fatigue influence of laser treated tool steel surface. Procedia Eng. 2014;74:429-42.
10. Reuter MA, van Schaik A, Gutzmer J, Bartie N, Abadías-Llamas A. Challenges of the circular economy: a material, metallurgical, and product design perspective. Annu Rev Mater Res. 2019;49(1):253-74.
11. Verma P, Saha R, Chaira D. Waste steel scrap to nanostructured powder and superior compact through powder metallurgy: powder generation, processing and characterization. Powder Technol. 2018;326:159-67.
12. Upadhyaya GS. Powder metallurgy technology. 1st ed. Cambridge: Cambridge International Science Publishing Ltd; 1998.
13. Zhang W, Hu Y, Zhang G, Wang Z. Formation of nanoscale metallic glassy particle reinforced Al-based composite powders by high energy milling. Metals. 2017;7(10):425-34.
14. Mendoza-Duarte JM, Estrada-Guel I, Carreño-Gallardo C, Martínez-Sánchez RL. Study of Al composites prepared by high energy ball milling: effect of processing conditions. J Alloys Compd. 2015;643:S172-7.
15. Suryanarayana C. Mechanical alloying and milling. Prog Mater Sci. 2001;46(1-2):1-184.
16. Ghasali E, Alizadeh M, Shirvanimoghaddam K, Mirzajany R, Niazmand M, Faeghi-Nia A, et al. Porous and non-porous alumina reinforced magnesium matrix composite through microwave and spark plasma sintering processes. Mater Chem Phys. 2018;212:252-9.
17. Ghasali E, Ebadzadeh T, Alizadeh M, Razavi M. Spark plasma sintering of WC-based cermets/titanium and vanadium added composites: a comparative study on the microstructure and mechanical properties. Ceram Int. 2018;44(9):10646-56.
18. Kuffner BHB, Silva G, Rodrigues CA, Rodrigues G. Study of the AISI 52100 steel reuse through the powder metallurgy route using high energy ball milling. Mater Res. 2018;21:1-10.
19. Claudiney M, Adhimar O, Daniela S, Patricia C, Vander R, Mateus J, et al. A new method to recycle stainless–steel duplex UNS S31803 chips. Metals. 2018;8(7):546-58.
20. Dias ANO, Silva A, Rodrigues CA, Melo MLNM, Rodrigues G, Silva G. Effect of high energy milling time of the aluminum bronze alloy obtained by powder metallurgy with niobium carbide addition. Mater Res. 2017;20(3):747-54.
21. Mahboubi Soufiani A, Enayati MH, Karimzadeh F. Fabrication and characterization of nanostructured Ti6Al4V powder from machining scraps. Adv Powder Technol. 2010;21(3):336-40.
22. Matos RAG, Mendes J, Kuffner BHB, Melo MLNM, Silva G. Evaluation of X22CrMoV12-1 alloy with vanadium carbide addition submitted to powder metallurgy. Mater Res. 2023;26:e20220237.
23. Bílek P, Sobotová J, Jurci P. Evaluation of the microstructural changes in Cr-V ledeburitic tool steel depending on the austenitization temperature. Mater Technol. 2011;45(5):489-93.
24. Zhou T, Spartacus G, Dahlström A, Babu RP, Davydok A, Hedström P. Computational thermodynamics and kinetics-guided re-engineering of a high-performance tool steel. Scr Mater. 2023;232:115496-500.
25. Bohler-Uddeholm. Vanadis 8® SuperClean [Internet]. 2023 [cited 2023 Apr 14]. Available from: https://www.uddeholm.com/brazil/pt-br/products/uddeholm-vanadis-8-superclean/
26. Mesquita RA, Barbosa CA. High-speed steels produced by conventional casting, spray forming and powder metallurgy. Mater Sci Forum. 2005;498-499:244-50.
27. Barbedo EL, Gonçalves PH, Lamoglia MS, Pontes AMP, Bastos Kuffner BH, Gomes GF, et al. Analysis of milling efficiency of the Vanadis® 8 tool steel with additions of vanadium and molybdenum carbides. Mater Res. 2021;24(5):e20210054.
28. Toboła D, Łętocha A. Influence of combined mechanical processes on tribological properties of tool steels Vanadis 8 and vancron 40 with a similar hardness. Front Mech Eng. 2021;7:1-11.
29. Langford JI, Wilson AJC. Scherrer after sixty years: a survey and some new results in the determination of crystallite size. J Appl Cryst. 1978;11(2):102-13.
30. ASTM: American Society for Testing and Materials. ASTM E09-09: standard test methods of compression testing of metallic materials at room temperature. West Conshohocken: ASTM; 2009.
31. ASTM: American Society for Testing and Materials. ASTM C20-22: standard test methods for apparent porosity, water absorption, apparent specific gravity, and bulk density of burned refractory brick and shapes by boiling water. West Conshohocken: ASTM; 2022.
32. Bakkal M, Shih AJ, McSpadden SB, Liu CT, Scattergood RO. Light emission, chip morphology, and burr formation in drilling the bulk metallic glass. Int J Mach Tools Manuf. 2005;45(7-8):741-52.
33. Chang I, Zhao Y. Advances in powder metallurgy: properties, processing and applications. 1st ed. Sawston: Woodhead Publishing; 2013.
34. Gheisari KH, Javadpour S, Oh JT, Ghaffari M. The effect of milling speed on the structural properties of mechanically alloyed Fe-45% Ni powders. J Alloys Compd. 2009;472(1-2):416-20.
35. Tornberg C, Fölzer A. New optimised manufacturing route for PM tool steels and high speed steels. In: 6th International Tooling Conference; 2002; Karlstad, Sweden. Proceedings. Karlstad: Karlstad University; 2002. p. 363-76.
36. Chang SH, Lee KY, Huang KT, Yang TH. Evaluation of the microstructure and properties of Cr_3C_2 powders added to Vanadis 4 alloy steel via vacuum sintering and thermal treatments. Kovove Mater. 2021;57(5):317-27.
37. Huang KT, Chang S-H, Yeh P-T. Microstructures and mechanical properties of TaC added to Vanadis 4 tool steel through vacuum sintering and thermal treatments. ISIJ Int. 2017;57(7):1252-60.

38. Dudina DV, Bokhonov BB. Materials development using high energy ball milling: a review dedicated to the memory of M.A. Korchagin. J Compos Science. 2022;6(7):188-204.
39. Suryanarayana C. Mechanical alloying: a critical review. Mater Res Lett. 2022;10(10):619-47.
40. Fernandes CM, Puga J, Senos AMR. Nanometric WC-12 wt% AISI 304 powders obtained by high energy ball milling. Adv Powder Technol. 2019;30(5):1018-24.
41. Gonzalez-Pociño A, Alvarez-Antolin F, Asensio-Lozano J. Optimization of quenching and tempering parameters for the precipitation of M_7C_3 and MC secondary carbides and the removal of the austenite retained in Vanadis 10 tool steel. Metals. 2019;9(6):627-37.
42. Sobotova J. Diagnostics of the microstructural changes in sub-zero processed Vanadis 6 P/M ledeburitic tool steel. Mater Technol. 2013;47:93-8.